J Electroceram (2009) 22:383–389
DOI 10.1007/s10832-007-9410-1

Chemical solution deposition of ferroelectric lead lanthanum zirconate titanate films on base-metal foils

Beihai Ma · Do-Kyun Kwon · Manoj Narayanan · U. (Balu) Balachandran

Received: 30 July 2007 / Accepted: 27 December 2007 / Published online: 10 January 2008
© Springer Science + Business Media, LLC 2008

Abstract Development of electronic devices with better performance and smaller size requires the passive components to be embedded within a printed wire board (PWB). The "film-on-foil" approach is the most viable method for embedding these components within a PWB. We have deposited high-permittivity ferroelectric lead lanthanum zirconate titanate ($Pb_{0.92}La_{0.08}Zr_{0.52}Ti_{0.48}O_x$, PLZT 8/52/48) films on base metal foils by chemical solution deposition. These prefabricated capacitor sheets can be embedded into PWBs for power electronic applications. To eliminate the parasitic effect caused by the formation of a low-permittivity interfacial oxide, a conductive buffer layer of lanthanum nickel oxide (LNO) was applied by chemical solution deposition on nickel foil before the deposition of PLZT. With a ≈0.7-μm-thick ferroelectric PLZT film grown on LNO-buffered nickel foil, we measured capacitance densities of 1.5 μF/cm^2, breakdown field strength $E_b >$ 1.2 MV/cm, and leakage current density of 2×10^{-8}A/cm^2. The dielectric relaxation current decay obeys the Curie-von Schweidler law, with exponent n=0.85 and 0.94 for PLZT grown directly on Ni and that grown on LNO-buffered Ni foils, respectively. When compared with samples deposited directly on Ni substrate, PLZT grown on LNO buffered Ni substrates exhibit slimmer hysteresis loop and better energy storage capability. With these desirable characters, PLZT film-on-foil capacitors hold particular promise for use in high-voltage embedded passives.

Keywords Ferroelectric film · PLZT · Ceramic capacitor · Dielectric property · Chemical solution deposition

1 Introduction

Embedding high-permittivity (high-κ) dielectrics into a low-temperature-processed printed wire board (PWB) is being investigated to replace discrete surface-mounted capacitors. Advantages of such devices include electronics miniaturization, greater device reliability, and manufacturing cost reduction. This technology also holds particular promise for applications that require high capacitance density and high volumetric efficiency, such as the power electronics in plug-in hybrid electric vehicles (PHEV). Because embedded capacitors can be located directly underneath active devices, they greatly reduce component footprint, dramatically shorten interconnect lengths, reduce parasitic inductive losses and electromagnetic interference, and allow operation at higher frequency. Further, reliability is improved because the number and size of interconnections are reduced, as solder joints that often are most susceptible to failure are no longer needed [1]. Photolithographic methods in combination with etching and metallization steps can be used to synthesize the needed capacitive elements and interconnections rapidly and in large quantity [2]. While this technology has primarily received attention for decoupling capacitors in microelec-

The submitted manuscript has been created by UChicago Argonne, LLC, Operator of Argonne National Laboratory ("Argonne"). Argonne, a U.S. Department of Energy Office of Science laboratory, is operated under Contract No. DE-AC02-06CH11357. The U.S. Government retains for itself, and others acting on its behalf, a paid-up nonexclusive, irrevocable worldwide license in said article to reproduce, prepare derivative works, distribute copies to the public, and perform publicly and display publicly, by or on behalf of the Government.

B. Ma (✉) · D.-K. Kwon · M. Narayanan · U. (B.) Balachandran
Energy Systems Division, Argonne National Laboratory,
Argonne, IL 60439, USA
e-mail: bma@anl.gov

tronic applications, it can also be extended to higher voltage applications.

Historically, the integration of high-κ dielectric materials into PWBs has been thwarted by the incompatibility of the respective processing conditions. Polymer layers in a PWB cannot withstand the high temperatures (600–800 °C) required for processing the ceramic dielectric films to obtain the desired crystalline structure. Many efforts have been made to reduce film growth temperatures. Unfortunately, these efforts significantly compromise the dielectric properties. The complex crystalline structures common to high-κ dielectric materials are intimately linked to their attractive dielectric properties. Development of these crystalline structures becomes extremely challenging, if not impossible, at reduced processing temperatures [3–5]. Recently, great success was achieved by a film-on-foil approach, where the dielectric was first deposited by chemical solution deposition (CSD) on a thin base metal foil, followed by crystallization at high temperatures. The coated foil was subsequently embedded into a PWB. Low-dissipation loss has been demonstrated in pre-fabricated ceramic film-on-foil capacitors with high capacitance density [6–9].

An additional challenge in developing high-κ film-on-foil capacitors is associated with the use of base metal foils. Since PWB applications are extremely cost competitive, the use of expensive noble metal materials must be minimized. The incorporation of less-expensive base metals with high-κ dielectric is challenging. The high firing temperatures and oxidizing atmospheres necessary for synthesis and densification of many oxides can be detrimental to oxidation-sensitive base metals, especially copper, whereas the reducing atmospheres that are favored by base metals can result in excessive defect concentrations and frustrated phase formation of the dielectric ceramic films [7, 10]. These effects lead to unsatisfactory dielectric performance for practical applications.

Two approaches have been taken to eliminate the deleterious effects of a low-κ parasitic oxide at the metal-dielectric interface, which acts as a series low-capacitance capacitor component and reduces the overall capacitance. In the first approach, the formation of an interfacial oxide is avoided by crystallizing the dielectric at a low oxygen partial pressure (pO_2) environment [8, 9]. The second approach is to negate the influence of the interfacial low-κ parasitic oxide by interposing a conductive oxide buffer layer between the dielectric ceramic film and the metal foil. The conductive oxide buffer layer acts effectively as the bottom electrode. And any isolated crystallites of secondary phase oxide formed between the dielectric ceramic film and the metal substrate will likely play an inactive role in the performance of the parallel-plate capacitor [11, 12]. While this approach requires the deposition of a second material, it can avoid the intricacies of low pO_2 processing.

The majority of research works have been directed to PLZT 6-9/65/35 (Zr/Ti ration is 65/35 and amount of doping of La is between 6 and 9%), which is near the morphotropic phase boundary (MPB) between ferroelectric rhombohedral phase (FE_{Rh}) and the ferroelectric tetragonal phase (FE_{Te}). Compositions near the MPB have been particularly important because most of the properties of interest are “maximized” along the phase boundary line. For example, in the PLZT 7/65/35 material, a quasi-ferroelectric phase (also known as penferroelectric phase [13]) exists in the temperature region between the Curie temperature and the metastable phase transition temperature (between 96 and 140 °C [14]). Although this material exhibits high dielectric constant and other desirable properties at room temperature, it has a low Curie temperature and, therefore, cannot be used for power electronic devices operate at moderately high temperature (up to 150 °C).

With high-temperature application bared in mind, we investigated PLZT thin films with compositions in the FE_{Te} region for higher Curie temperature and more tolerable synthesis conditions. In this paper, we present our recent results on fabrication and property of $Pb_{0.92}La_{0.08}Zr_{0.52}Ti_{0.48}O_x$ (PLZT 8/52/48) films on base-metal substrates which are applicable to high-voltage embedded passives. These PLZT film-on-foil capacitors can then be embedded in PWBs. This particular composition has been chosen for study because of its potential applicability for moderately high temperature (up to 150 °C) applications such as for use in the power electronics for plug-in hybrid electric vehicles. We report the film processing conditions and their effects on the dielectric properties of CSD-processed PLZT on nickel (Ni) foils and the use of $LaNiO_3$ (LNO) buffer layers for improving the dielectric performance of the PLZT 8/52/48 film-on-foil capacitors.

2 Experimental procedure

Nickel (ESPI Metals, 99.98% pure) foils with 500-μm thickness were diamond polished to 1-μm finish for use as substrates. Prior to being coated, the polished Ni foils were ultrasonic cleaned with acetone and then methanol. LNO precursor solutions (0.2 M) were prepared by dissolving lanthanum nitrate and nickel acetate in 2-methoxyethanol and refluxing for 2 h. Precursor solution was spin coated onto Ni foil substrates at 3,000 rpm for 30 s with a Laurel WS400 spin coater. Spin-coated films were pyrolyzed at 450 °C for 15 min and subsequently annealed at 575–650 °C for 2–15 min with a final anneal for an additional 1 h. All annealing and pyrolysis were done in air. This process was repeated to deposit LNO films of thickness between 0.15 and 0.6 μm (1 and 4 coatings) for subsequent deposition of $Pb_{0.92}La_{0.08}Zr_{0.52}Ti_{0.48}O_x$ films.

$Pb_{0.92}La_{0.08}Zr_{0.52}Ti_{0.48}O_x$ (PLZT 8/52/48) precursor solutions (0.5 M) were prepared by a modified 2-methoxyethanol synthesis route [12] using lead acetate trihydrate, titanium isopropoxide, zirconium *n*-propoxide, and lanthanum nitrate. It contains 20% excess lead to compensate the loss during heat treatment process. The solution was spin coated at 3,000 rpm on bare or LNO-buffered Ni foils, pyrolyzed at 450 °C for 10 min, and subsequently annealed at 650 °C for 2–5 min, with a final anneal at 650 °C for 20 min to ensure complete transformation to the perovskite phase. All annealing and pyrolysis were done in air. Solution coating and firing were repeated to produce films of desired thicknesses.

Thermogravimetric analysis (TGA) and differential thermal analysis (DTA) were conducted to investigate phase formation in LNO precursor. X-ray diffraction (XRD) was conducted to study phase development in the processed films. The surface roughness of the films was measured by atomic force microscopy (AFM) using a Digital Instruments D3000 scanning probe microscope operated in the tapping mode. The microstructure was characterized by scanning electron microscopy (SEM) using a Hitachi S-4700-II field-emission electron microscope. Cross-sectional SEM was performed on samples prepared with a focused ion beam (FIB) at the Electron Microscopy Center (EMC) at Argonne National Laboratory. Platinum (Pt) top electrodes with thicknesses of 100 nm were deposited by electron-beam evaporation through a shadow mask to define ≈250-µm-diameter capacitors. Electrical measurements were taken on the Pt/PLZT/(LNO)/Ni heterostructure by contacting a Pt top electrode pad and the Ni substrate (bottom electrode). Dielectric properties were determined by using an HP 4192A impedance analyzer with a 0.1-V oscillating signal at 10 kHz. Leakage current and breakdown field strength were measured with a Keithley 237 high-voltage power source meter. Hysteresis loops were measured with a Radiant RT600HVAS high-voltage test system.

3 Results and discussion

PLZT films directly deposited on polished Ni foils were phase pure with no preferred crystallographic orientation. No cracking or delamination occurred even with PLZT films as thick as 5.8 µm. Although interfacial secondary phases were not detectable by cross-sectional SEM, the reduced relative permittivity (≤400) suggested that a detrimental interfacial layer might exist when compared with PLZT thin films deposited on platinum-electrode-bearing silicon substrates using similar deposition conditions. These films had a relative permittivity of 1,500. The thickness-dependent apparent permittivity was analyzed by using a series capacitor model. The results indicated an interfacial capacitance resulting from a low-κ interfacial layer, as well as a suppressed bulk permittivity due to diffusion between the PLZT and Ni substrate [12]. To reduce these deleterious effects, we explored use of a conductive LNO buffer layer.

Results from thermogravimetric analysis (TGA) and differential thermal analysis (DTA) for the LNO precursor solution are plotted in Fig. 1. An exothermic peaks is visible at 305 °C on the DTA curve due to the evaporation of water and combustion of metal organic, respectively. Weight losses were observed on the TGA curve corresponding to these exothermic peaks. The TGA curve indicated a further weight loss starting at 575 °C, which is related to the conversion of amorphous into crystalline LNO phase [15]. These results were used to determine the crystallization temperature for treating the LNO films. Several LNO films with various numbers of coatings were deposited on Ni foils and annealed at 575–650 °C in air. After pyrolysis and crystallization, each layer of LNO coating leads to a film thickness of 0.15 µm. SEM microstructure observations revealed that 2–3 coatings are necessary to achieve a complete coverage of the Ni foil by LNO.

Figure 2 shows X-ray diffraction patterns from films pyrolyzed at 450 °C for 10 min and annealed at different temperatures for 2 min. Formation of a nickel oxide interfacial layer can be discerned even at the lowest annealing temperature, and its extent increases with increasing temperature. However, the nickel oxide crystallites are likely dispersed within the LNO, which is highly conductive and connected to the Ni substrate underneath. Therefore, the LNO film, along with the Ni substrate underneath, serves as the bottom electrode and prevents the parasitic influence of the interfacial nickel oxide. Phase-

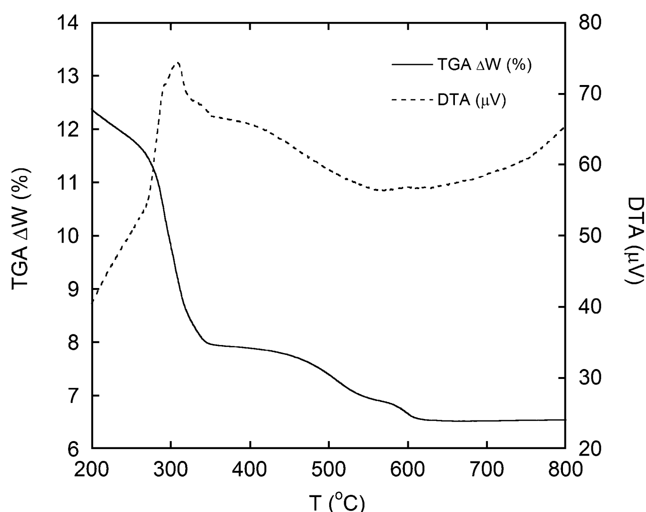

Fig. 1 DTA and TGA curves of LNO precursor measured between 200 and 800 °C in air

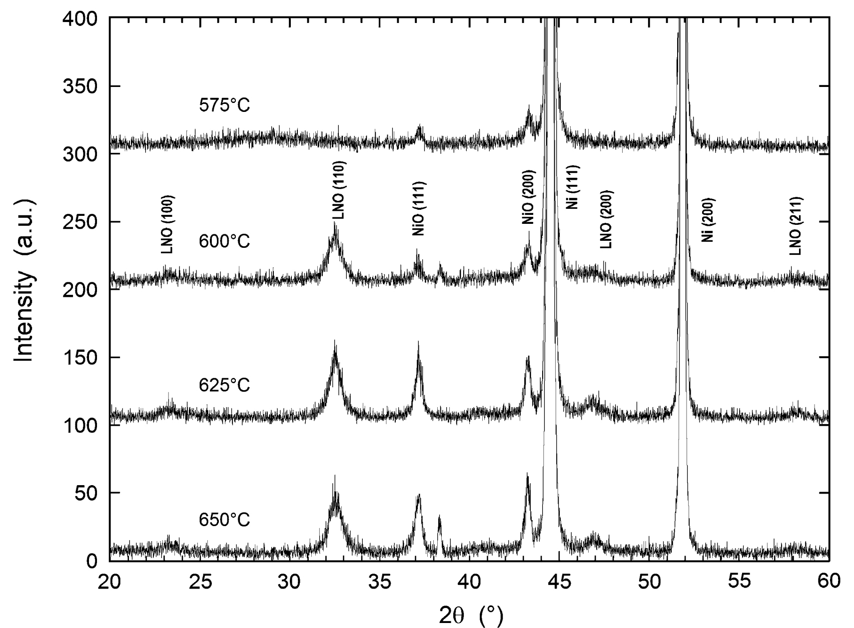

Fig. 2 XRD patterns of 0.45-μm-thick LNO films annealed at various temperatures

pure LNO films with a slight (110) out-of-plane preferred orientation begin crystallizing at ≈600 °C. Based on surface roughness and film density, an annealing temperature of 650 °C for treating LNO was chosen for studies of PLZT/LNO/Ni foil capacitors.

Samples of 0.7-μm-thick PLZT were grown on LNO-buffered Ni substrates to investigate the effect of LNO layer thickness on dielectric performance. The relative permittivity of these samples is shown in Fig. 3. Here, the variable is the number of LNO layers. A single layer of LNO coating averts the parasitic influence of interfacial nickel oxide formation and significantly improves the relative permittivity. More complete coverage and planarization are needed for reduced dielectric loss (<5%). With three or more layers of LNO coating, we measured a relative permittivity of > 1120 on samples of 0.7-μm-thick PLZT grown on LNO-buffered Ni foils. The film-on-foil PLZT/LNO/Ni capacitors exhibit capacitance densities of ≈1.5 $\mu F/cm^2$, which is close to the 1.7 $\mu F/cm^2$ value obtained with platinized Si substrates.

Figure 4 shows the root-mean-square (RMS) surface roughness measured by AFM for polished Ni foil and the terminal surface RMS roughness of LNO with one to four coatings. The LNO buffer layer improves the terminal surface smoothness for subsequent growth of the PLZT layer. Also shown in Fig. 4 is the breakdown field strength of 0.7-μm-thick PLZT grown on top of various thickness of LNO-buffered Ni substrates. The breakdown field strength

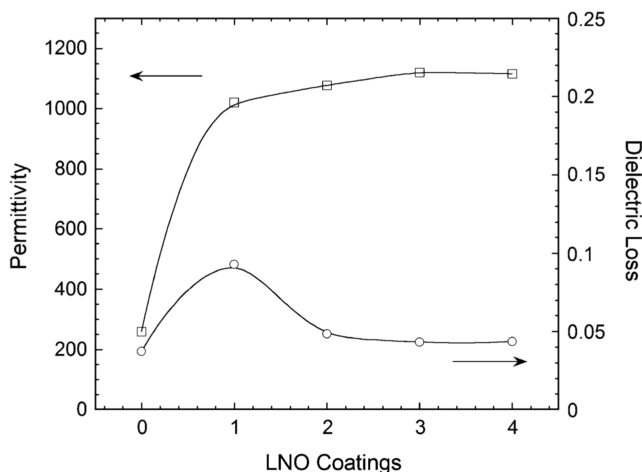

Fig. 3 Dielectric properties of 0.7-μm-thick PLZT films grown on LNO-buffered Ni substrates with various numbers of LNO coatings

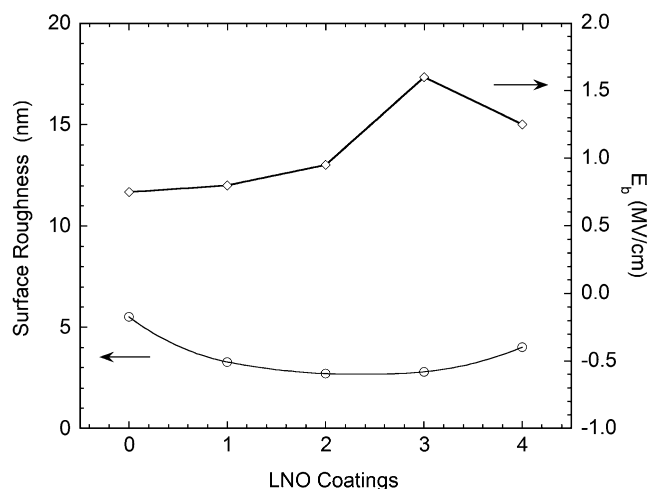

Fig. 4 Surface roughness and breakdown field strength of 0.7-μm-thick PLZT as a function of the number of LNO coatings

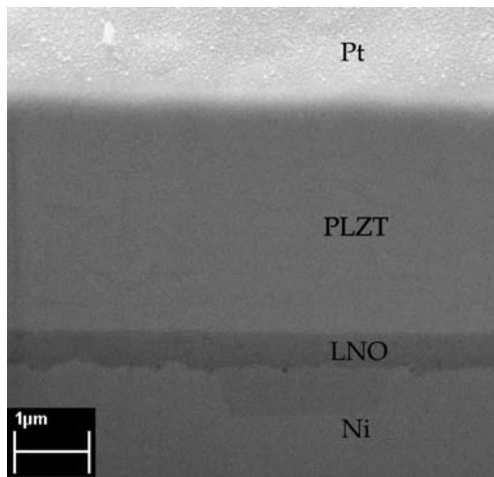

Fig. 5 Cross-sectional SEM of a PLZT/LNO/Ni film-on-foil heterostructure

was >1.2×10^6 V/cm on a PLZT grown on three-layer-LNO-buffered Ni foil that was 0.45-μm thick. LNO film metrology exerted a pronounced influence on PLZT breakdown strength. Two to three coatings of LNO were required to form a layer that completely covered and ameliorated the roughness of the polished Ni foil. More than three coatings of LNO again lead to moderate increase in terminal surface roughness due to excessive film thickness and grain growth caused by recurring heat treatment.

The planarizing influence of the LNO layer is highlighted in the cross-sectional SEM image of a heterostructure PLZT (≈3.5 μm)/LNO (≈0.45 μm)/Ni foil, as shown in Fig. 5. Besides obviating any NiO formation along the Ni interface, the LNO provides a smooth interface for PLZT nucleation and growth. The PLZT film grown on LNO-buffered Ni foil is dense as no discernable porosity can be observed. The smooth interfaces and dense microstructure both contribute to the higher breakdown strengths.

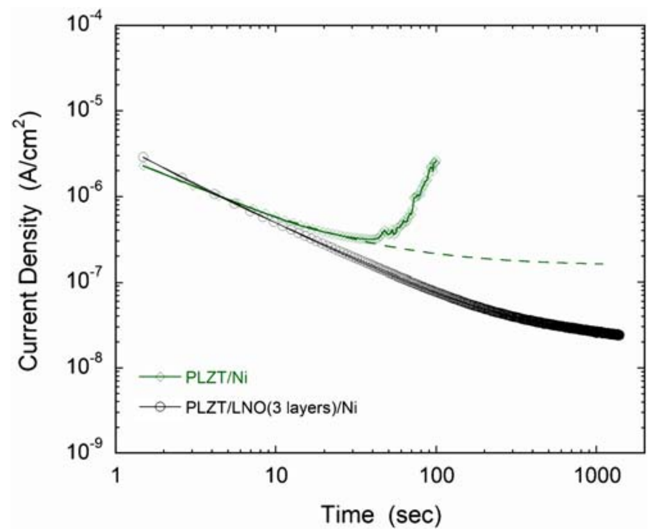

Fig. 7 Dielectric relaxation current of PLZT film-on-foil samples with and without LNO buffer

Figure 6 shows the current density as a function of applied voltage across the top and bottom electrodes measured on two PLZT film-on-foil samples. Voltage was increased in 0.5-V increments, and the current was measured with a 1-s delay. These two samples were processed under similar conditions, except that one was grown directly on Ni foil and the other was grown on 0.45-μm-thick (three layers) LNO buffered Ni foil. Leakage current for the sample with LNO buffer is over one order of magnitude smaller than that measured on the sample grown directly on Ni foil. This may suggest a higher charge carrier concentration or possibly change in electronic structure caused by nickel diffusion in the PLZT films deposited directly on Ni substrate when compared with that grown on LNO buffered Ni substrates. Once again, this finding demonstrated the

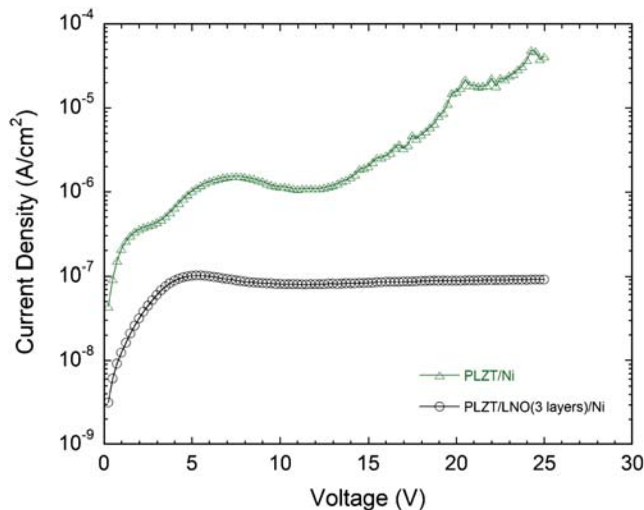

Fig. 6 Current density as a function of applied voltage for PLZT film-on-foil samples with and without LNO buffer

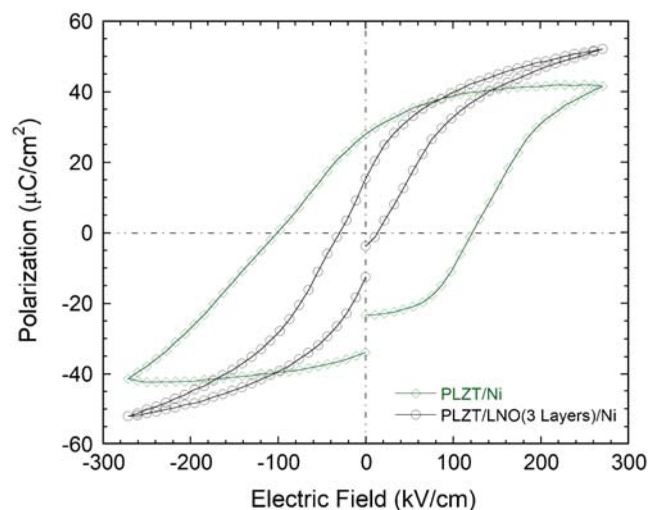

Fig. 8 *P–E* hysteresis loops of PLZT film-on-foil samples grown on nickel substrates with and without LNO buffer

pronounced influence of LNO buffer on the properties of PLZT film-on-foil capacitors grown on Ni foils.

Figure 7 shows the dielectric relaxation current for these two samples measured under a constant bias voltage of 10 V (corresponding to an applied electrical field ≈140 kV/cm) across the top and bottom electrodes. The measurements were conducted by keeping the top Pt electrode positive and the bottom Ni electrode grounded. Both curves showed strong initial time dependence, indicating depolarization effects. However, after the initial decrease in current, sample grown directly on Ni foil exhibited degradation behavior leading to breakdown in approximately 50 s, whereas sample grown on 0.45-μm-thick LNO-buffered Ni foil showed no sign of degradation after 1000 sec. The dielectric relaxation current decay obeys the Curie-von Schweidler law [16–18],

$$J = J_s + J_0 \cdot t^{-n} \qquad (1)$$

where J_s is the steady-state current density, J_o is a fitting constant, t is relaxation time in seconds, and n is the slope of the log-log plot. There are three possible mechanism associated with the Curie-von Schweidler law: space charge trapping, relaxation time distribution, and electrical charge hopping. Fitting data to Eq. 1, we found n values of 0.85 and 0.94 for PLZT film-on-foil capacitor grown directly on Ni and that grown on 0.45-μm-thick LNO buffered Ni foils, respectively. Fitting curves are plotted as dashed lines in Fig. 7. Leakage current densities of 2×10^{-7} A/cm^2 and 2×10^{-8} A/cm^2 were determined for ferroelectric PLZT films grown on bare and LNO buffered Ni foils, respectively.

Figure 8 shows the P–E hysteresis loops of two PLZT film-on-foil samples grown on nickel substrates with 0.45-μm-thick LNO buffer and that without LNO buffer. Both samples were measured under electric field ≈275 kV/cm (corresponds to an applied voltage of 20 V). When compared to that without LNO buffer, the *P–E* hysteresis loop for the sample with LNO buffer is much slimmer and exhibits higher value of spontaneous polarization (P_s). These are desirable characteristics for energy storage applications. The remnant polarization (P_r) values were measured at 27.5 and 14.7 μC/cm^2, and the coercive electric field (E_c) values were 104 and 28.6 kV/cm, for PLZT film deposited directly on Ni and that deposited on 0.45-μm-thick LNO buffered Ni substrates, respectively. Smaller P_r and E_c values are likely resulted from the decrease in oxygen vacancies in the PLZT film [19]. Because adding La^{3+} as a donor-dopant to substitute Pb^{2+} can suppress the creation of oxygen vacancies according to the following equation.

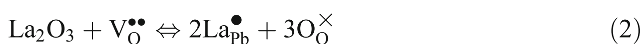

$$La_2O_3 + V_O^{\bullet\bullet} \Leftrightarrow 2La_{Pb}^{\bullet} + 3O_O^{\times} \qquad (2)$$

Whereas in the samples of PLZT deposited directly on Ni substrates without a LNO buffer, in addition to the formation of parasitic interfacial nickel oxide phase, Ni from the substrate may likely diffuse into PLZT film to cause the following possible scenarios: (1) consume La and form $LaNiO_3$, (2) incorporate into grain boundaries in PLZT, or (3) substitute B-site ions in the PLZT material. For the first case, the effective La doping level would have reduced and concentration of oxygen vacancy would increase based on Eq. 2; for the second case, incorporation of Ni into grain boundary would lead to an increased electronic conductivity, i.e., higher current and lower equivalent series resistance (ESR); and for the third case, substitution of B-site ions by Ni would again increase oxygen vacancies in PLZT. All processes would lead to an increase in charge carriers (oxygen vacancies and electrons) in the material. This explains why a fatter hysteresis loop was observed on the sample without a LNO buffer. As shown in Figs. 6 and 7, higher leakage current and low ESR are also evident for PLZT deposited on Ni without LNO buffer when compared with the sample with LNO buffer. These may also attribute to higher concentration of charge carriers in the film.

4 Conclusions

PLZT film-on-foil capacitors have been grown on bare and LNO buffer Ni foils. The LNO acts as the bottom electrode, obviating any parasitic low-permittivity interfacial NiO formation that would reduce the overall capacitance. This LNO layer allows the film-on-foil capacitors to be processed in air without the intricacies incurred by low pO_2 processing. The LNO also compensates the roughness of the Ni foil and provides a smooth interface for the PLZT films, resulting in higher breakdown strengths. For a ≈0.7-μm-thick ferroelectric PLZT film grown on LNO-buffered nickel foils, we observed capacitance densities of 1.5 μF/cm^2, breakdown field strength >1.2 MV/cm, and leakage current density of 2×10^{-8}A/cm^2. The decay in the dielectric relaxation current obeys the Curie-von Schweidler law, with n=0.85 and 0.94 for PLZT grown directly on Ni and that grown on LNO buffered Ni foils, respectively. When compared with samples deposited directly on Ni substrate, PLZT grown on LNO buffered Ni substrates exhibit slimmer hysteresis loop and better energy storage capability. With these desirable characters, PLZT film-on-foil capacitors hold particular promise for use in high-voltage embedded passives.

Acknowledgments Work funded by the U.S. Department of Energy, Office of FreedomCAR and Vehicle Technologies, under Contract DE-AC02-06CH11357. This work benefited from the use of the Electron Microscopy Center (EMC) at Argonne National Laboratory. The authors thank Dr. R. E. Koritala at EMC for her assistance with SEM.

References

1. W. Borland, M. Doyle, L. Dellis, O. Renovales, D. Majumdar, Mater. Res. Soc. Symp. Proc. **833**, 143 (2005)
2. D. Nelms, R. Ulrich, L. Schaper, S. Reeder, Proceedings of the 48th IEEE Electronic Components and Technology Conference, pp. 247–251, Institute of Electrical and Electronic Engineers, Piscataway, NJ (1998).
3. W. Zhang, K. Sasaki, T. Hata, Jpn. J. Appl. Phys., Part 1. **35**, 5084 (1996)
4. Y. Zhu, J. Zhu, Y.J. Song, S.B. Desu, Appl. Phys. Lett. **73**, 1958 (1998)
5. J.T. Dawley, P.G. Clem, Appl. Phys. Lett. **81**, 3028 (2002)
6. J. Ihlefeld, B. Laughlin, A. Hunt-Lowery, W. Borland, A. Kingon, J.P. Maria, J. Electroceramics. **14**, 95 (2005)
7. T. Kim, J.N. Hanson, A. Gruverman, A.I. Kingon, S.K. Streiffer, Appl. Phys. Lett. **88**, 262907 (2006)
8. M.D. Losego, L.H. Jimison, J.F. Ihlefeld, J-P. Maria, Appl. Phys. Lett. **86**, 172906 (2005)
9. A.I. Kingon, S. Srinivasan, Nature Materials. **4**, 233 (2005)
10. S.Y. Kim, D.J. Kim, J.G. Hong, S.K. Streiffer, A.I. Kingon, J. Mater. Res. **14**, 1371 (1999)
11. Q. Zou, H.E. Ruda, B.G. Yacobi, Appl. Phys. Lett. **78**, 1282 (2001)
12. D.Y. Kaufman, S. Sabha, K. Uprety, Proceedings of the 12th US-Japan Seminar on Dielectric and Piezoelectric Ceramics, pp. 305–308, Annapolis, MD (November 2005)
13. Y. Xu, *Ferroelectroc Materials and Their Applications* (Elsevier Science Publishing Company, New York, 1993), pp. 164–168
14. H.M. O'Bryan Jr., J. Am. Ceram. Soc. **56**, 385 (1973)
15. D. Bao, X. Yao, N. Wakiya, K. Shinozaki, N. Mizutani, J. Phys. D. Appl. Phys. **36**, 1217 (2003)
16. P. Curie, Ann. Chim. Phys. **18**, 203 (1889)
17. E. von Schweidler, Ann. Phys. **24**, 711 (1907)
18. K. Jonscher, *Dielectric Relaxation in Solids* (Chelsea Dielectrics Press, London, 1983)
19. M.V. Raymond, J. Chen, D.M. Smith, Integ. Ferroelectrics. **5**, 73 (1994)